minerals

MDPI

Article

Potential Pathways of Critical Elements in Fe–Ni Laterites: Insights from Skyros Island (Greece)

Christos Kanellopoulos [1] and Maria Economou-Eliopoulos [2,*]

[1] Hellenic Survey of Geology & Mineral Exploration, Sp. Loui 1, Olympic Village, 13677 Acharnai, Greece; ckanellopoulos@gmail.com
[2] Department of Geology and Geoenvironment, National and Kapodistrian University of Athens, 15784 Athens, Greece
* Correspondence: econom@geol.uoa.gr

Highlights

- Origin of compact magnetite hosted in ultramafic sequence of ophiolite complexes.
- Texture features and mineral chemistry distinguishing metamorphosed Fe–Ni laterites from altered chromite ores.
- Pathways of critical metals from weathered ultramafic rocks to metamorphosed Fe–Ni laterites.

Abstract

The occurrence of compact magnetite within peridotites of Skyros Island (Greece) has been recorded, but its origin is still uncertain. Since critical metals (Ni, Co, Sc, PGE, REE) are a growing concern on a worldwide scale and may provide evidence for the origin of ores, their investigation in magnetite ore is the objective of the present investigation. The determination of major and trace elements in representative compact magnetite from Skyros and their detailed investigation using SEM/EDS provide some evidence of genetic significance. The presence of pisolitic–oolitic texture, chromite fragments in a spatial association, with a composition ranging from high-Al to high-Cr, and flat-shaped PGE patterns indicates the origin of compact magnetite ore by metamorphism of Fe–Ni laterites rather than alteration of chromite ore. Critical elements hosted in primary minerals of ophiolites during chemical and mechanical weathering are released easily, and subsequently they are incorporated into secondary minerals and are redistributed during subsequent re-deposition and metamorphism. The relatively low content of critical elements in Skyros compact magnetite may be related to low content in the source/ parent ophiolites and re-deposition of laterite crusts onto peridotites, suggesting a lack of a pH contrast at the base (lack of carbonates) to facilitate their precipitation.

Keywords: Fe–Ni laterite; re-deposition; critical elements; spinel; rare earth elements; platinum-group elements

Check for updates

Academic Editors: Hermann Kudrass and Liqiang Yang

Received: 11 September 2026
Revised: 23 October 2026
Accepted: 29 October 2026
Published: 1 November 2026

Copyright: © 2026 by the authors. Licensee MDPI, Basel, Switzerland. This article is an open access article distributed under the terms and conditions of the Creative Commons Attribution (CC BY) license.

1. Introduction

Compact magnetite of hydrothermal origin in ophiolite complexes is a widespread mineral, in association with apatite at tectonic contacts between a gabbroic rock and peridotites, in the form of dykes within basalts or in association with Fe–Cu–Ni–Co sulfides hosted in ultramafic rocks, as well as Ti-magnetite of magmatic origin in cumulate gabbro of the magmatic sequence [1–7]. The compact magnetite ore consisting mainly of magnetite

surrounding chromite cores within peridotites in Olympos, Skyros (Stefanies or Peramata) and other ophiolites of northern Greece has been interpreted as magmatic, following the crystallization of chromite, but the origin of massive magnetite ore within ultramafic rocks of ophiolite complexes has not been established yet [4].

The mineralization associated with ophiolites in Skyros Island, like chromite, has been studied extensively [8–10]. However, the origin of compact magnetite within peridotites in the area of Stefanies or Peramata (Skyros) and compact magnetite fragments dispersed in the areas of Atsitsa, Agios Ioannis and Agia Alexandra of Skyros (Figure 1), probably coming from exploration for metals during the Second World War, is still unclear [4,11]. Although the dominant component of the massive ore from the above areas of Skyros is magnetite, some characteristics of Fe–Ni laterites have been identified as well. Since pseudo-autochthonous Fe–Ni deposits derived by the transportation and re-deposition of initial laterite crusts on peridotites are well known in the Balkan Peninsula [12–16], the location of compact magnetite occurrences within peridotites has been re-examined and re-interpreted recently [16]. Also, critical metals, such as platinum-group elements (PGE), rare earth elements (REE), nickel (Ni), cobalt (Co), and scandium (Sc), are a growing concern on a worldwide scale [17] and may provide evidence for the origin of ores; their investigation is a major topic of the present work. The objective of the present study is the analysis of representative compact magnetite samples for major and trace element composition, including critical elements [REE, PGE, Ni, Co, Sc; mineral chemistry and scanning along a back-scattered electron image of minerals. The principal contribution is an integrated reassessment of ore genesis and the potential pathways of critical metals to compact magnetite hosted in peridotites of ophiolite complexes.

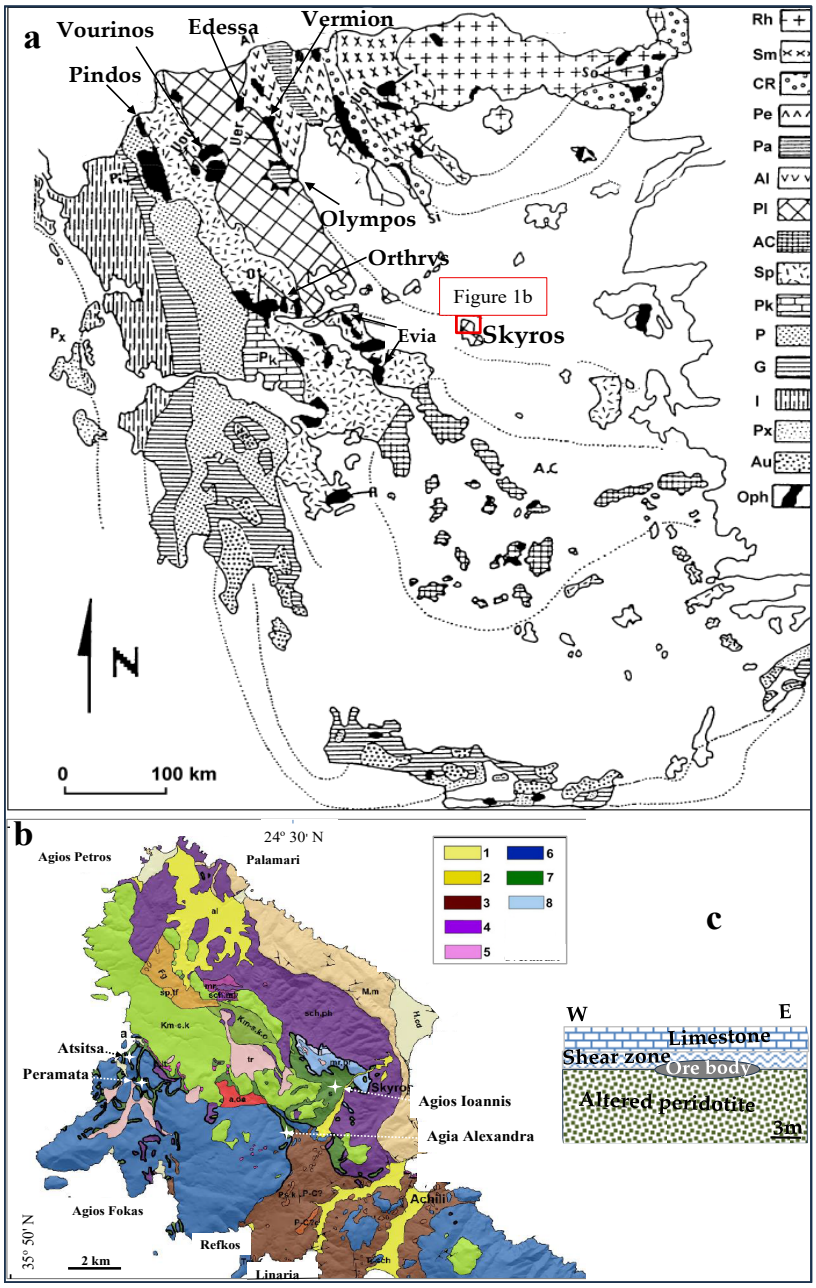


Figure 1. Simplified map of the geotectonic zones of the Hellenides showing the main ophiolite complexes of Greece, such as Orthrys, Vourinos, and Pindos. Symbols: Oph = ophiolites; Rh = Rhodope zone; Sm = Serbo–Macedonian Massif; CR = Circun–Rhodope zone; (Pe, Pa, Al) = Axios zone; Pl = Pelagonian zone; AC = Attico–Cycladic zone; Sp = Pindos zone; P = Parnassos–Giona zone; G = Gavrovou–Tripolis zone; I = Ionian zone; Px = Pakson zone (after Mountrakis, 1992) [18]. Metamorphosed Fe–Ni laterites are located to the east of the Pelagonian massif (Vermion, Edessa, Olympos and Skyros). (**a**) Simplified geological map of Skyros Island showing the major structural elements of Greece; (**b**) modified after [19]. Numbers: 1: Quaternary sediments; 2: upper Miocene–lower Pliocene sediments; 3: Miocene volcanics; 4: limestones and flysch; 5: ophiolites; 6: upper metamorphic unit; 7: lower metamorphic unit; 8: sub-Pelagonian unit of NW Skyros. The symbol ✦ shows the sampling sites of magnetite-bearing ores (**b**); representative geological section, showing the schistose ore geometry, contact with peridotite from the area of Stefanies or Peramata (**c**).

2. Materials and Methods

2.1. Sampling

Forty (40) thin-polished sections prepared from magnetite occurrences on Skyros were examined by transmitted and reflected light microscopy using a Zeiss Axioskop 40 optical microscope (Carl Zeiss MicroImaging GmbH, Göttingen, Germany), then carbon-coated and examined using a scanning electron microscope (SEM) JEOL JSMIT500 SEM instrument (JEOL USA, Inc., Peabody, MA, USA) equipped with an Oxford 100 Ultramax analytical device (Oxford Instruments, Abingdon, UK). The metamorphosed Fe–Ni laterite samples were collected from small occurrences, from the area of Peramata or Stefanies (coordinates: 38° 54′ N and 24° 27′ E), while those from Agios Ioannis, Agia Alexandra and Atsitsa were not in situ (Figures 1 and 2). A minimum of two kg of samples was necessary for bulk analyses to approximate statistical homogeneity.

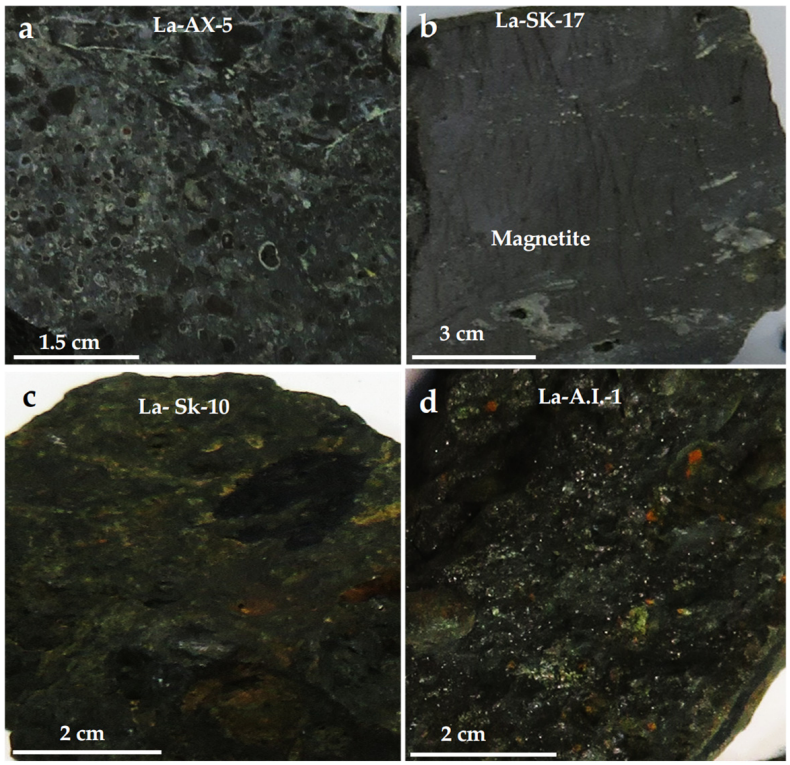


Figure 2. Photographs of hand samples showing multiple stages of pisolite-oolite development of metamorphosed Fe–Ni laterite samples from Stefanies or Peramata, Agia Alexandra and Agios Ioannis (**a**,**c**,**d**), and compact magnetite (**b**) of Skyros Island. The observed spherical silicate assemblages are a characteristic feature.

2.2. Analytical Methods

The geochemical analyses were conducted for major elements by X-ray Fluorescence (XRF; S4 Pioneer BRUKER AXS; Billerica, MA, USA) and the analyses for trace elements were conducted by Inductively Coupled Plasma–Mass Spectrometry (ICP-MS; Perkin-Elmer SCIEX ELAN 6100; Waltham, MA, USA). For the bulk rock geochemical analyses, the samples were pulverized to <200 mesh in an agate mill. For ICP–MS analysis, aliquots of the pulverized samples were digested using an HCl–HNO_3–HF acid mixture. The geochemical analyses were performed in the laboratories of the Hellenic Survey of Geology and Mineral Exploration.

Carbon (C) and sulfur (S) contents were determined by combustion followed by infrared detection using a LECO CS230 Carbon/Sulfur Determinator (LECO Corpora-

tion, St. Joseph, MI, USA) in the laboratories of the Hellenic Survey of Geology and Mineral Exploration.

Examination of carbon-coated polished thin sections from the laterite samples was carried out at the Hellenic Survey of Geology & Mineral Exploration, using a JEOL JSMIT500 SEM instrument (JEOL USA, Inc., Peabody, MA, USA) equipped with an Oxford 100 Ultramax analytical device (Oxford Instruments, Abingdon, UK). Backscattered-electron imaging, element-distribution mapping, and point analyses were processed using AZtec software (version 6.0; Oxford Instruments NanoAnalysis, High Wycombe, UK). Analyses were performed at 20 kV accelerating voltage and 1.5–5 nA beam current, beam diameter < 1 μm, and with energy calibration against pure Co. The X-ray lines used for elemental identification and quantification included: OsMα, PtMα, IrMα, AuMα, AgLα, AsLα, FeKα, NiKα, CoKα, CuKα, CrKα, AlKα, TiKα, CaKα, SiKα, MnKα, MgK, EuLα, ClKα.

Platinum-group element analyses were carried out using the Ni-sulfide fire-assay preconcentration technique, with the nickel fire-assay technique from large (30 g) samples at Genalysis Laboratory Services, Perth, Australia. This method allows for complete dissolution of samples. The detection limits were 2 ppb for Os, Ir, Ru, Pt, and Pd, 1 ppb for Rh, and 5 ppb for Au. The SARM7 sample was used as a standard.

3. Geological Outline

The Fe–Ni laterite deposits in Greece are associated with ophiolites, remnants of the Tethyan oceanic lithosphere, and are mostly allochthonous, redeposited as marine sediments, and buried by later sedimentary rocks [12,13]. Skyros ophiolites (Figure 1) are mainly associated with the Eohellenic Nappe ophiolitic mélange and comprise highly consisting of serpentinized harzburgites, gabbroic rocks, dolerites, tholeiitic basaltic lavas have been determined as late Jurassic–early Cretaceous [19–22]. Small (1 m × 10 m) lens-like redeposited Fe–Ni laterite occurrences at E. Vermion, metamorphosed to amphibolite facies, have been studied [4,15]. The tectonostratigraphic analysis of the formations related to the tectonic emplacement of the Hellenic ophiolites has shown an older age of ophiolite obduction from its external to its internal part of the Hellenides. Specifically, the timing for Skyros ophiolites (Figure 1b) has been determined as late Jurassic–early Cretaceous of the Vardar/Axios terrane [23,24].

An elongate, small (4 m × 7 m) lens of compact magnetite, near the contact with Cretaceous limestone, was found within peridotite near the contact with Cretaceous limestone, parallel to the thrust movement of a shearing zone (Figure 1c). Exploration for metals by excavation of surficial exposures left behind dispersed laterite fragments. Reserve tonnage is unknown. A common characteristic of all samples studied is their compact texture, the occurrence of pisolite-oolites, and the presence of chromite relics. In addition, they have been reworked due to repeated marine transgression and regression, deposited in a shallow marine environment, and affected by thrust faulting (Figures 1c and 2a–d).

4. Results

4.1. Mineralogical Characteristics

4.1.1. Chromite and Magnetite

Clastic chromite grains, inherited from the parent ophiolitic rocks of varying composition from high-Cr to high-Al (Figure 3; Table 1), and the presence of pisolitic–oolitic texture within magnetite ore (Figures 2 and 4) are salient features supporting the laterite origin, despite its occurrence within peridotite. Detrital angular and rounded fragments of chromite are widespread within oolites and matrix, often showing a porous texture. Elevated Mn

contents, which reach the highest values (up to 6.2 wt.% MnO) at grain boundaries, and Zn contents (up to 2.1 wt.% ZnO) are common in Fe-chromite (Table 1; Figure 5).

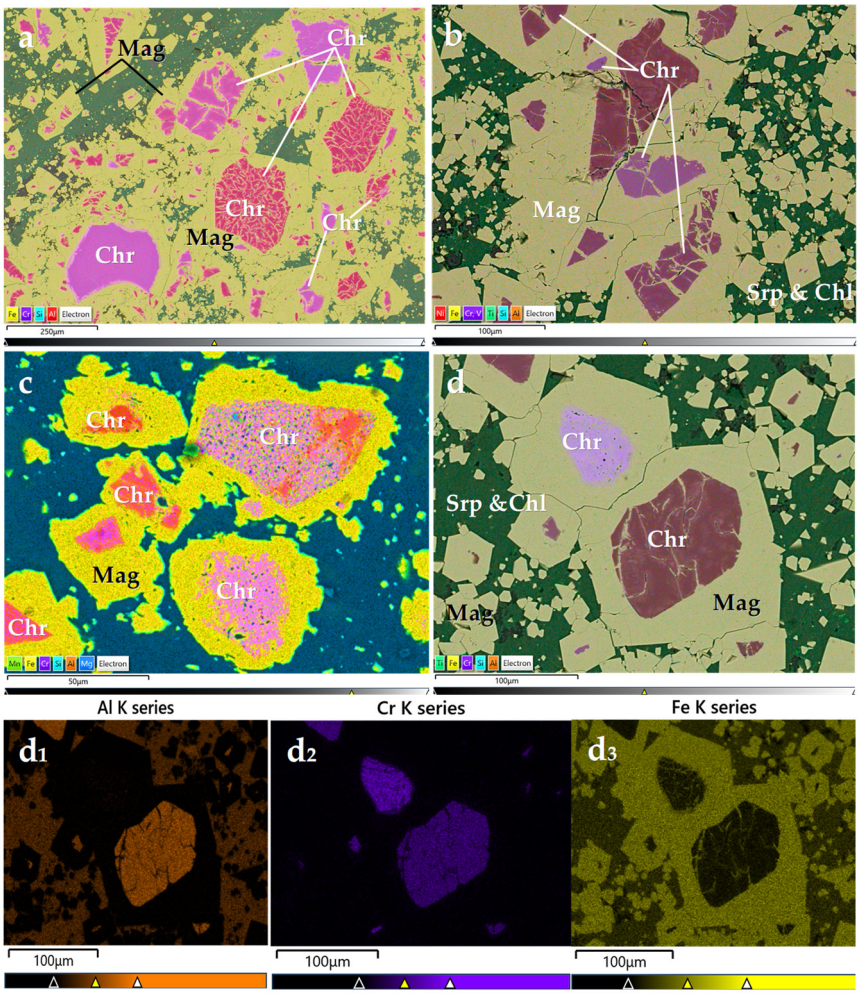


Figure 3. Selected color back-scattered electron images (BSEI) of metamorphosed Fe–Ni laterite from Skyros, showing the wide compositional variation of chromite (**a**–**d**) and the porous texture of chromite grains (**c**). X-ray elemental maps ($\mathbf{d_1}$–$\mathbf{d_3}$), showing differences in the intensity of color/composition. Abbreviations: Chr = chromite; Mag = magnetite; Srp = serpentine; Chl = chlorite.

Table 1. Representative electron SEM–EDS analyses of chromite cores, Fe-chromite rims and pure magnetite from the Skyros magnetite ore. Abbreviation: n.d. = not detected.

	Chromite											
Wt.%												
SiO_2	0.2	n.d.	n.d.	n.d.	n.d.	n.d.	n.d.	n.d.	n.d.	n.d.	n.d.	n.d.
TiO_2	n.d.	0.2	n.d.	n.d.	n.d.	n.d.	n.d.	n.d.	n.d.	n.d.	0.2	n.d.
Al_2O_3	7.6	15.1	33.2	14.1	14	24.7	24.2	16.8	34.2	23.1	17.5	26.6
Cr_2O_3	64.1	54.8	36	57	57.5	44.5	44.1	52.9	36	47.6	51.1	43.3
V_2O_5	n.d.	0.3	n.d.	n.d.	n.d.	0.3	n.d.	0.3	0.3	n.d.	n.d.	n.d.
Fe_2O_3	n.d.	n.d.	0.5	n.d.	n.d.	0.9	1.2	2.6	1.2	2.6	2.1	0.7
FeO	19.0	18.3	15.8	18.7	18.5	17.7	16.7	15.2	16.9	14.9	16.5	17.2
MnO	n.d.	n.d.	n.d.	n.d.	n.d.	n.d.	n.d.	n.d.	n.d.	0.3	0.4	0.5
MgO	6.7	9.3	13.8	10.2	9.4	12.4	12.3	13.2	14.3	13.4	11.5	12.2
ZnO	0.4	0.3	0.4	n.d.	0.5	n.d.	n.d.	0.4	0.3	n.d.	n.d.	n.d.
Total	**98.0**	**98.3**	**99.7**	**100**	**99.9**	**100.5**	**98.5**	**101.4**	**103.2**	**101.9**	**99.3**	**100.5**

Table 1. *Cont.*

	Chromite											
	Fe-chromite										Mag-netite	
Wt.%												
SiO_2	0.4	n.d.	0.8	n.d.	n.d.	0.9	n.d.	n.d.	n.d.	n.d.	n.d.	0.6
TiO_2	n.d.	n.d.	n.d.	n.d.	n.d.	0.5	0.5	n.d.	n.d.	n.d.	n.d.	n.d.
Al_2O_3	13.5	15.1	17.7	34	25.7	1.2	n.d.	2.3	1.6	n.d.	n.d.	0.7
Cr_2O_3	43.8	46.5	32.1	30.6	43.8	44.3	43.9	50.5	51.5	n.d.	n.d.	n.d
V_2O_5	n.d.	n.d.	0.3	0.3	0.3	0.8	0.7	n.d.	0.3	n.d.	n.d.	n.d.
Fe_2O_3	9.7	6.1	16.3	4.3	0.5	18.4	18.3	16.3	14.5	67.4	67.0	66.8
FeO	26	26	26	18.3	23	23.5	24.6	22.0	27.8	30.3	30.2	28.9
MnO	2.5	1.9	2.3	0.4	0.4	5.8	5.5	6.2	6.1	n.d.	n.d.	0.4
MgO	4.3	4.1	4.5	12.5	9.2	2.3	n.d.	2.0	1.8	n.d.	n.d.	0.7
ZnO	0.6	0.4	1.6	0.4	0.3	2.0	2.1	1.1	1.0	n.d.	n.d.	n.d.
Total	**100.8**	**100.1**	**101.6**	**100.8**	**103.2**	**98.7**	**95.6**	**100.4**	**104.6**	**97.7**	**97.2**	**98.1**

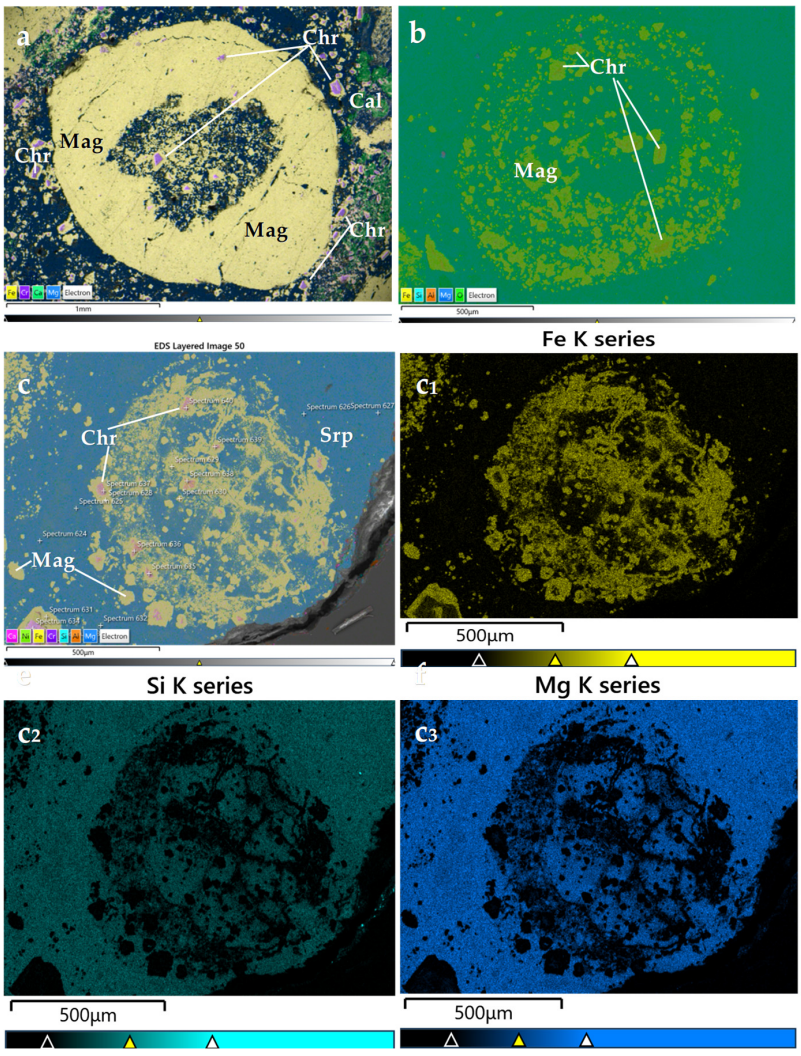


Figure 4. Selected color back-scattered electron images (BSEI) of metamorphosed Fe–Ni laterite from Skyros, showing pisolitic–oolitic texture and the presence of abundant chromite within the matrix and oolites themselves (**a**–**c**); X-ray elemental maps (**c$_1$**–**c$_3$**), showing differences in the intensity of color/composition. Magnetite occurs either as rims surrounding chromite cores, as large crystals without chromite cores, or as fine-grained magnetite. Abbreviations: As those in Figure 3.

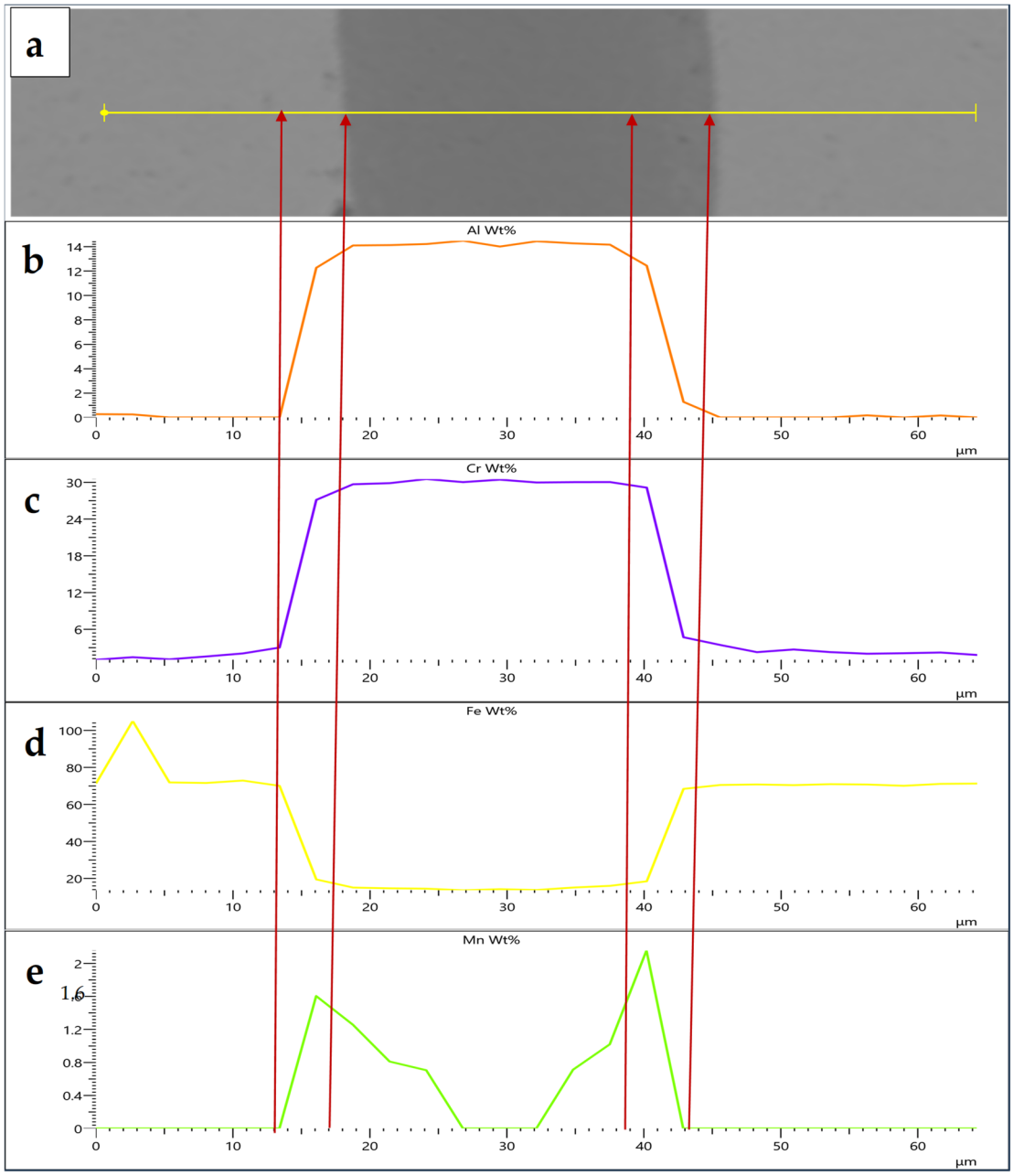


Figure 5. Scanning along a back-scattered electron image of zoned chromite showing relatively unaltered chromite core and Fe-enriched rim (**a**); the variation of Al, Cr, Fe, and Mn (**b**–**e**) highlights elevated Mn content at the periphery of a Fe-chromite, whereas within magnetite rim and chromite core it is negligible.

Magnetite occurs either as rims surrounding chromite cores, as large crystals without chromite cores, or as fine-grained (Figures 3 and 4). The gradual stacking of magnetite of varying density, shifting towards more compact ore (a few centimeters in size), was located in the area of Stefanies or Peramata (Figures 1c and 2b). Compact magnetite within such a small ore occurrence, along with a shearing zone with strong schistose peridotite, is pure (Table 1; Figure 2b). It is commonly associated with serpentine (Figure 6; Table 2) located in a matrix of various silicates (chlorite, serpentine, diopside, garnet).

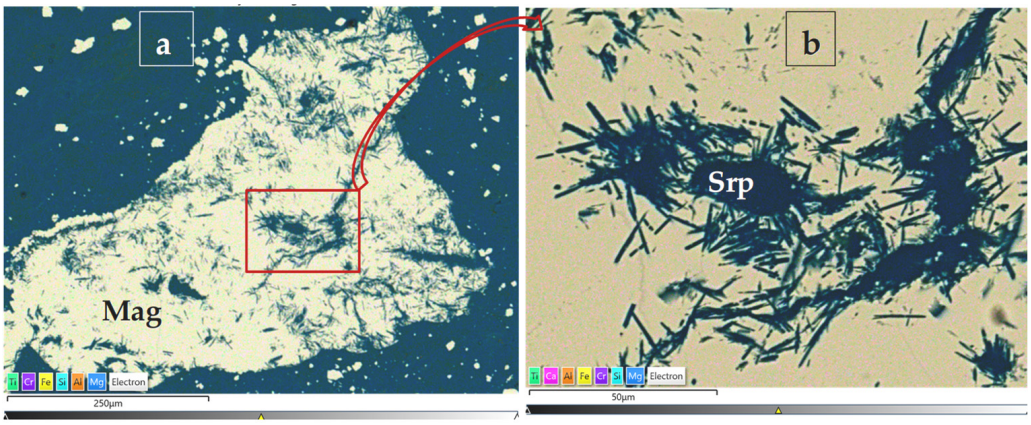


Figure 6. Pure magnetite concentrations associated with serpentine within metamorphosed laterite, (**a**); Enlarged figure (**b**). Abbreviations: Mag = magnetite; Srp = serpentine.

Table 2. Representative SEM/EDS analyses of silicates from the Skyros magnetite ore.

wt.%	Srp	Srp	Ni-Srp	Chl	Grt	Grt	Grt	Grt	Di	Di	Di
SiO_2	42.2	41.1	39.7	34.2	32.8	32.6	33.1	37.0	54.6	54.6	54.3
TiO_2	n.d.	n.d.	n.d.	n.d.	8.2	7.3	6.3	n.d.	n.d.	n.d.	n.d.
Al_2O_3	1.9	1.7	0.9	11.1	0.2	n.d.	1.1	1.8	n.d.	n.d.	n.d.
Cr_2O_3	1	n.d.	n.d.	0.4	0.8	1.0	1.1	0.8	n.d.	n.d.	n.d.
FeO	4.2	4.1	5.4	7.6	18.6	22.8	21.5	25.4	5.5	2.0	4.0
MgO	39.2	38.0	3.9	32.0	0.5	n.d.	0.5	n.d.	16.2	18.7	15.5
NiO	n.d.	0.2	27.7	0.9	n.d.	n.d.	n.d.	n.d.	0.2	n.d.	n.d.
MnO	n.d.	n.d.	0.2	0.2	n.d.	n.d.	n.d.	n.d.	0.5	n.d.	0.3
CaO	n.d.	n.d.	0.9	n.d.	34.7	33.1	33.1	33.8	24.2	25.6	26.2
Sc_2O_3	n.d.	n.d.	n.d.	n.d.	n.d.	n.d.	0.3	0.3	n.d.	n.d.	n.d.
Total	**88.5**	**85.1**	**78.7**	**86.4**	**95.8**	**96.8**	**97.0**	**99.1**	**101.2**	**100.9**	**100.3**
wt.%	**Chl**	**Chl**	**Chl**	**Fe-Chl**	**Fe-Chl**	**Srp**	**Srp**	**Srp**	**Srp**	**Srp**	**Srp**
SiO_2	34.6	34.2	35.6	24.9	25.5	41.8	39.1	38.1	37.0	36.8	36.8
TiO_2	n.d.	n.d.	n.d.	n.d.	0.13	n.d.	n.d.	n.d.	n.d.	n.d	n.d
Al_2O_3	12.8	11.3	10.8	17.0	18.6	1.7	4.1	5.6	7.3	6.9	7.8
Cr_2O_3	0.6	1.5	1.9	0.5	1.3	0.4	0.7	1.1	1.0	1.2	0.5
FeO	9.3	6.7	4.6	38.1	28.1	3.3	3.4	4.6	4.5	5.6	4.6
MgO	31.1	32.6	34.8	5.1	10.0	37.7	35.9	36.1	36.4	36.1	36.0
NiO	1.0	0.8	0.6	2.3	4.1	0.5	0.6	0.4	0.3	0.2	n.d.
MnO	0.2	0.2	n.d.	n.d.	0.9	n.d.	n.d.	n.d.	0.1	0.1	n.d.
Total	**89.6**	**87.3**	**88.3**	**87.9**	**88.6**	**85.4**	**83.8**	**85.9**	**86.6**	**86.9**	**85.7**

Abbreviations: Srp = serpentine; Grt = garnet; Chl = Chlorite; Di = Diopside; n.d. = not detected.

4.1.2. Silicates and Sulfides

The groundmass of magnetite ore is fine-grained and is composed mostly of magnetite, coarser clastic grains of chromite and silicates. Abundant silicate minerals include serpentine, chlorite, diopside, garnet, calcite, quartz, alloys, and base metal sulfides (Figure 7). Nickel and Co are mostly hosted into newly formed Fe–Ni–Co sulfides, like pentlandite and Co-bearing pentlandite (Figure 8; Table 3).

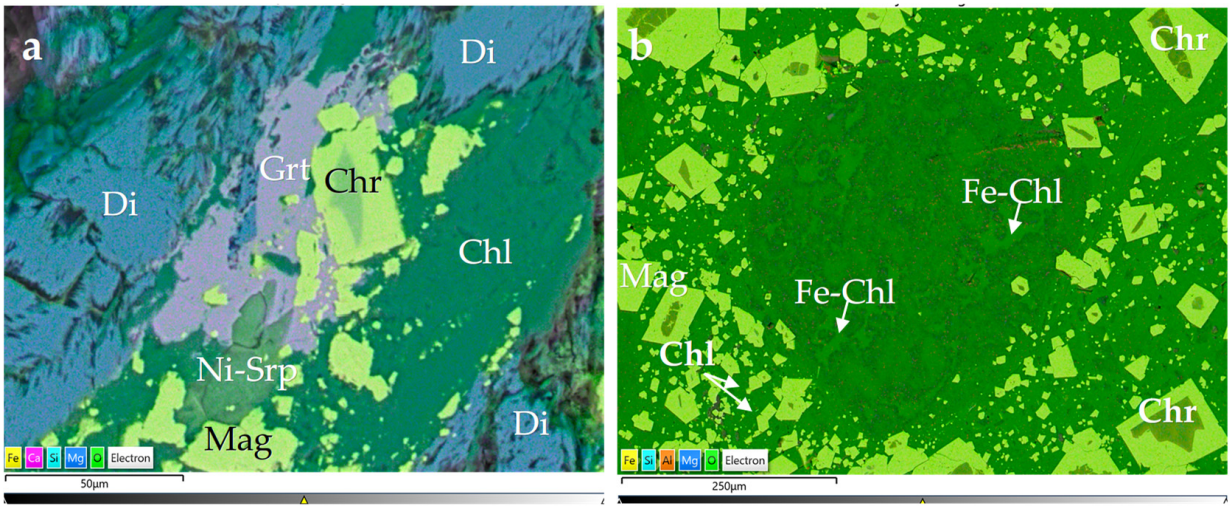


Figure 7. Selected color back-scattered electron images (BSEI) of metamorphosed Fe–Ni laterite from Skyros revealing texture relationships. The earlier formation and dominance of diopside compared with intergrowths of garnet, chlorite, and Ni-serpentine associated with chromite and magnetite (**a**). The composition of chlorite ranges from low Fe content in the matrix to Fe-elevated within spherical concentrations (**b**) (Figure 2; Table 2). Abbreviations: Mag = magnetite; Chr = chromite; Di = diopside; Ni-Srp = nickel-bearing serpentine; Grt = garnet; Chl = chlorite; Fe-Chl = iron-bearing chlorite.

Table 3. Representative SEM–EDS analyses of base metal minerals from the Skyros magnetite ore. Abbreviation: n.d. = not detected; Pn = pentlandite; Co-Pn = Co-bearing pentlandite.

I.D.	Co-Pn	Co-Pn	Co-Pn	Co-Pn	Pn	Pn	Pn
Fe	18.7	19.1	6.9	26.8	1.7	1.5	7.8
Co	17.6	18.3	4.6	14.9	n.d.	n.d.	n.d.
Ni	32	31.3	57.2	29.5	71.5	58.6	65.0
Cr	0.3	0.5	n.d.	n.d.	n.d.	n.d.	n.d.
S	31.1	31.3	30.2	26.8	26.6	39.9	25.7
Total	**99.7**	**100**	**98.9**	**98.0**	**99.8**	**100**	**98.5**

A characteristic feature of pentlandite in the matrix of magnetite is its high Co content (Table 3).

4.2. Geochemical Characteristics

Whole-rock analyses of Fe–Ni laterite occurrences from Skyros, including REE, PGE, and other critical elements, are provided (Table 4). In general, the trace element contents (Co, Ni, Sc, REE and PGE) in compact Fe–Ni laterites from Skyros Island are comparable to those from Northern Greece (E. Vermion, Edessa and Olympos) and relatively low compared with those of karst-type allochthonous laterites of the Balkan Peninsula [13,15]. In addition, average contents (n = 4) of magnetite separates from Skyros metamorphosed laterites showed 6500 ppm Ni, 14,600 ppm Cr, 280 ppm Cu, 270 ppm Zn, 290 ppm V and 8 ppm Sc [4].

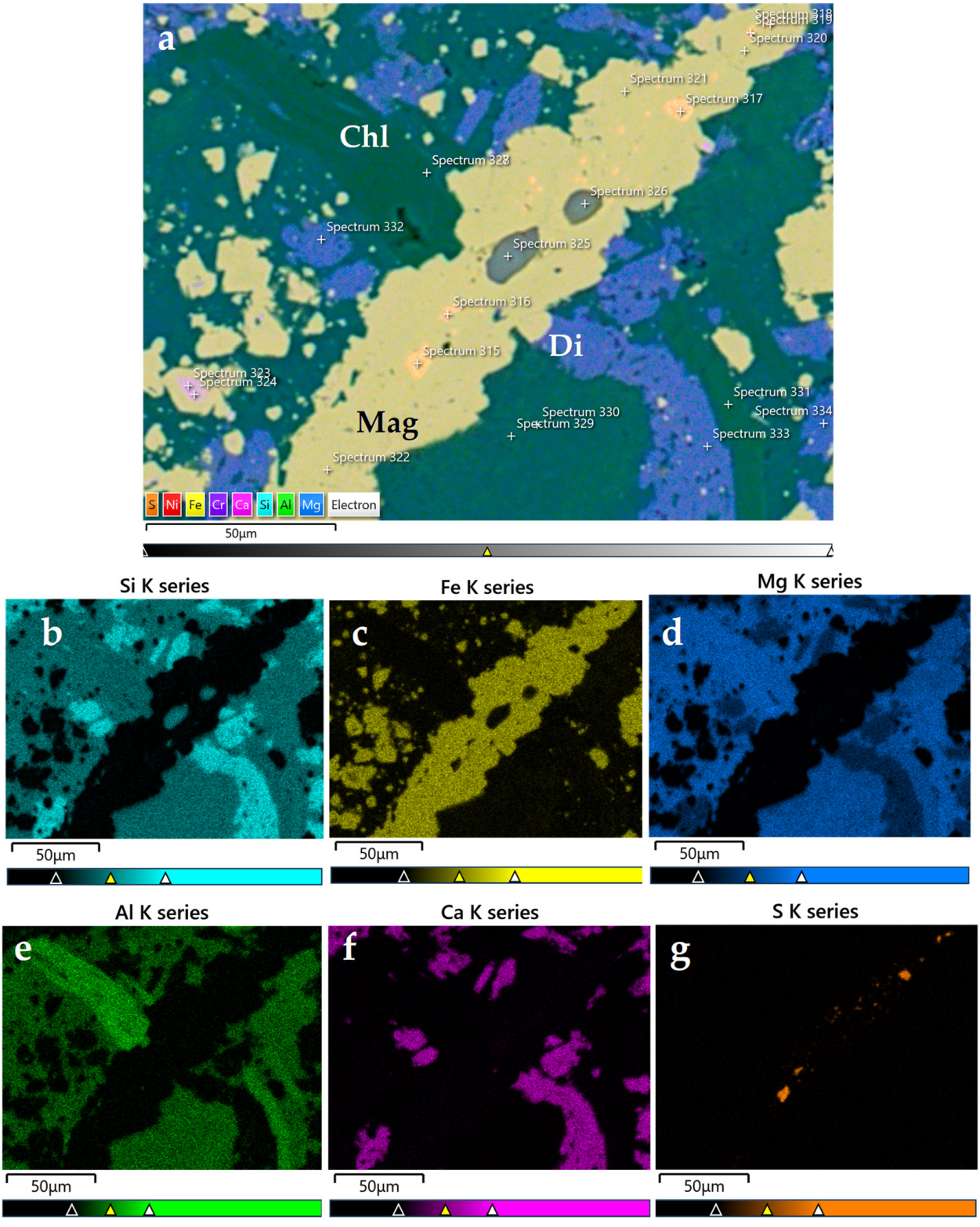


Figure 8. Color back-scattered electron image (BSEI) of metamorphosed Fe–Ni laterite from Skyros (**a**). X-ray elemental map, showing differences in the intensity of color/composition for minerals (**b**–**g**). Abbreviations: Co-Pn = Co-bearing pentlandite (provisional assignment); Pn = pentlandite; Mag = magnetite; Chl = chlorite; Srp = serpentine; Di = diopside.

Table 4. Representative analyses for major and trace elements of metamorphosed laterite occurrences from Skyros Island, Greece. Symbol: n.a. = not available.

				Agios		Agia
		Peramata or Stefanies		Ioannis	Atsita	Alexandra
	Altered	Metamorphosed	Pure	Pure Metamophosed		
	Peridotite	Laterite	Magnetite		Laterites	
	SK.M.9	La.Ax5	Sk-4-17	La AI.1	La Sk.1	La Sk10
Wt.%						
SiO_2	39.28	21.33	5.02	18.85	13.27	19.02
TiO_2	0.03	0.17	0.02	0.22	0.18	0.22
Al_2O_3	2.74	11.14	1.01	10.62	9.06	10.66
Fe_2O_3(t)	19.26	40.14	82.59	52.63	69.26	49.13
MnO	0.32	0.25	0.3	0.14	0.34	0.14
MgO	24.64	24.06	11.03	11.30	6.99	14.74
CaO	10.27	2.91	0.02	4.26	n.d.	3.62
Na_2O	n.d.	n.d.	n.d.	n.d.	n.d.	n.d.
K_2O	n.d.	n.d.	n.d.	0.01	n.d.	n.d.
P_2O_5	0.01	0.01	0.01	0.03	0.01	0.03
S	0.06	0.06	0.3	<0.06	<0.06	0.04
C	0.2	<0.06	<0.06	<0.06	<0.06	<0.06
LOI	3.14	n.d.	n.d	1.93	0.89	2.43
Total	**96.88**	**100.00**	**100.00**	**98.07**	**99.11**	**97.57**
ppm						
Ni	3200	6210	250	7700	8050	7200
Cr	2300	10,000	1300	7500	8500	7300
Co	210	210	65	430	320	440
Cu	10	25	5200	10	5	9
Zn	70	90	100	110	65	95
Sc	34	52	56	60	50	56
Li	2.0	5.0	<1	12	15	6
V	50	200	15	180	150	180
As	260	10	24	10	3.0	910
Ba	4300	25	1700	60	25	85
Zr	20	85	2.0	40	10	40
Y	2.5	5.0	8.0	8.0	2.0	8.0
Pb	10	5.0	10	6.0	6.0	10
Nb	20	35	8.0	41	40	45
Sn	20	35	30	20	15	15
Sb	5.0	0.8	20	5.0	20	80
La	82	8.0	9.0	14	3.0	9.0
Ce	8.9	13	12	20	5.0	12
Pr	<1	1.5	2.0	3.0	<1	2.0
Nd	4.0	6.0	7.0	9.0	2.0	7.0
Sm	<1	1.0	2.0	2.0	1.0	2.0
Eu	<1	<1	<1	<1	<1	<1
Gd	<1	1	2.0	2.0	<1	2.0
Tb	<1	<1	1.1	<1	<1	<1
Dy	<1	<1	2.0	2.0	<1	2.0
Ho	<1	<1	<1	<1	<1	<1
Er	<1	<1	1.5	1.5	<1	1
Tm	<1	<1	<1	<1	<1	<1

Table 4. *Cont.*

				Agios		Agia
		Peramata or Stefanies		Ioannis	Atsita	Alexandra
	Altered Peridotite	Metamorphosed Laterite	Pure Magnetite	Pure Metamophosed	Laterites	
	SK.M.9	La.Ax5	Sk-4-17	La AI.1	La Sk.1	La Sk10
Yb	<1	<1	1.0	1.5	<1	<1
Lu	<1	<1	<1	<1	<1	<1
Th	2.0	4.0	4.0	13	1.5	4.0
ppb						
Os	n.a.	n.a.	6	10	n.a.	3.5
Ir	n.a.	n.a.	4	30	n.a.	4.3
Ru	n.a	n.a	22	48	n.a	8.6
Rh	n.a.	n.a.	5	9.8	n.a.	9.4
Pt	n.a.	n.a.	2	48	n.a.	10
Pd	n.a	n.a	7	22	n.a	25
Au	n.d.	n.a.	7100	14	n.a.	5.0
UMIA	25.6	53.1	83.9	67.6	79.5	63.4
Ce/Ce*	0.26	1.02	0.81	0.96	1.10	0.58

Ce/Ce*= (2Ce/Ce chondrite)/(La/La chondrite + Nd/Nd chondrite).

Based on major components in ultramafic rocks and their behavior during the weathering process, an Ultramafic Index of Alteration (UMIA) has been used recently by [25]:

$$UMIA = [(Al_2O_3 + Fe_2O_{3t})/(Al_2O_3 + Fe_2O_{3t} + MgO + SiO_2)]*100 \text{ (in molar ratios)}$$

The calculated values of the UMIA for Skyros laterites range between 53.1 and 79.5 (Table 4). Calculated Ce anomalies [26] showed Ce/Ce* values ranging from 0.58 to 1.1. (Table 4). The small concentrations of pure magnetite differ in terms of lower Cr content, consistent with the rare presence of chromite grains, lower Ni, Co, Ti, Al, V, and PGE, and higher Cu, Au, and S contents.

The chondrite-normalized PGE patterns for metamorphosed Fe–Ni laterites from Skyros (Figure 9a) are comparable to those for laterites from major laterite deposits of Greece [27], but they differ from those from Olympos in terms of the negative slope of the latter (Figure 9b).

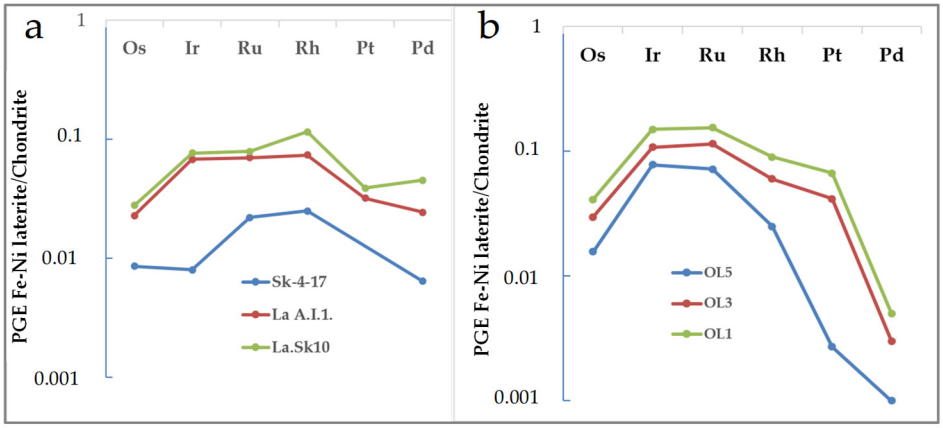


Figure 9. Chondrite-normalized PGE patterns for metamorphosed Fe–Ni laterites from Skyros (**a**) and Olympos (**b**). Data sources: Present study (**a**); [28] (**b**).

5. Discussion

5.1. Origin of Compact Magnetite and Potential Pathways of Critical Metals

Compact magnetite hosted by peridotites near its contact with overlying sediments can potentially preserve evidence of an earlier re-deposited laterite, while the potential pathways of critical elements, such as PGE, REE, Sc, Ni and Co, may be related to processes of element depletion and enrichment during a multistage geological evolution of ophiolites and associated laterites [4,14–16,29–34].

5.2. Critical Metals During 1st State of Weathering of Ultramafic Rocks

During the first stage of ophiolitic ultramafic rocks, Ni and Co are released from olivine, pyroxenes, or serpentine and are transported down the laterite profile. Cobalt is concentrated in Mn-(oxyhydr)oxides due to their affinity. Nickel is transferred further down into the deeper saprolite zone, replacing Mg^{2+} within the structure of Mg silicates. Scandium, after leaching from primary pyroxenes, is concentrated by replacing iron in goethite lattices (similar ionic radius to Fe^{3+}) or is adsorbed onto the surface of secondary Fe-Mn oxides [15,29–34]. In general, the REE content released from REE-depleted ophiolitic ultramafic rocks is low compared with those from felsic rocks, and they are incorporated in secondary minerals or absorbed by organic matter [34,35]. Also, Pt and Pd can be released during the weathering of ophiolites into weathered crusts. Average PGE content in separates from schlieren ores covering the whole Vourinos ophiolite complex (Greece) has shown 160 ppb PGE_{total}, 25 ppb Pt and 2,6 ppb Pd for chromite separates and 82 ppb PGE_{total}, 2.5 ppb Pt and 2.5 ppb Pd for silicate separates [36]. The elevated PGE contents, reaching up to 90 ppb Pt and 186 ppb Pd recorded in the Fe–Ni laterites of the Balkan Peninsula compared with parent ultramafic ophiolitic rocks [27], support the mobility of Pt and Pd.

5.2.1. 2nd Stage of Transportation, Re-Deposition in Shallow Sea Environments and Diagenesis

A salient feature of re-deposited laterites is the abundance of organic matter that is a major controlling factor of metal mobility and redistribution, due to a transformation into more mobile species through complexation with organic matter in low-pH rainwater [37–39]. During the stage of transportation and re-deposition, Sc, as a highly immobile cation (Sc^{3+}) under typical surface conditions, remains structurally bound within iron oxides. Instead, Ni and Co, as mobile ions, are leached. Cobalt, due to a chemical affinity for manganese, is mainly precipitated along with Mn-(oxyhydroxides), under favorable redox and alkalinity (pH) conditions. Iron oxyhydroxides are the main Ni-carrier and, to a lesser extent, Co [29–31].

The role of the Eh–pH conditions, due to the activity of micro-organisms, has been highlighted to enhance the PGE and REE mobility and re-deposition [15,29,30,37–41]. In general, Pt and Pd are soluble and can be transferred. The higher solubility and mobility of Pd compared with those of Pt, reflected in the higher value of the Pt/Pd ratio, has been established in many allochthonous laterite deposits [15]. Also, the extensive presence of total organic matter at the contact of the Lokris (Greece) allochthonous laterite deposit and the carbonate basement creates the appropriate conditions for REE leaching and re-deposition, up to 6000 ppm total REE [42]. The identification of a (La, Nd, Y) (CO_3)F member of the bastnaesite group associated with Al–Ni silicates in association with bacteriomorphic goethite may indicate REE remobilization by bio-leaching and re-precipitation on karstified limestone under alkaline and reducing conditions [42]. In contrast, allochthonous laterites overlying peridotite basement, like the case of Skyros laterites (Figure 1c), are fundamentally depleted in REE. Thus, the precipitation of dissolved REE in downward-migrating fluids is not facilitated due to the lack of a pH contrast at the base (alkaline neutralization boundary).

5.2.2. 3rd Stage of Metamorphism

A characteristic feature of metamorphosed Fe–Ni laterite occurrences in Skyros is the transportation of hydrated iron oxides into compact magnetite. Since these laterites inherit their composition mostly from the residual weathering of underlying ultramafic bedrock, the resulting magnetite preserves high concentrations of immobile Ni, Cr, and Co, and is depleted in REE. The magnetite from Skyros differs from compact magnetite of replacement or alteration origin in terms of the relict textures of surface processes, such as oolites and pisolites (Figure 4) in the former and elevated contents in V, Ti and REE contents in the latter [3].

Nickel and Co are mobilized and re-precipitated into newly formed Fe–Ni–Co sulfides, like pentlandite and Co-bearing pentlandite (Figure 8; Table 3), or substitute Mg in the chromite lattice [28]. The preference of Ni and Co in sulfides hosted in magnetite may indicate a limited capacity of magnetite to hold Ni and Co in its crystal structure under certain metamorphic conditions. Recently, Teitler et al. [43] indicated that during progressive metamorphic Fe^{3+} reduces to Fe^{2+}, the oxide lattice forces the structural entrapment of available Sc^{3+}, resulting in Sc partitioning into silicate phases like garnets, as exemplified by the presence of Sc (0.3 wt.% Sc) in garnet (Table 2). The presence of tetra-auricuprite (AuCu) and graphite within compact magnetite from Skyros [44] may reflect reducing microenvironments too, while sperrylite ($PtAs_2$) suggests its resistance to the evolution conditions. In addition, a combination of macroscopic textural characteristics, mineral chemistry, and geochemical signatures provides evidence distinguishing a metamorphosed laterite from an altered chromitite. The preserved oolitic/ pisolitic texture after metamorphism of Skyros re-deposited laterites, and the presence of clastic chromite fragments showing a wide compositional variation (Table 1) are consistent with a sedimentary origin. Also, Mg-dominant silicates as a major component of altered chromitites are not a mineralogical feature of the Skyros metamorphosed laterites (Table 3). In addition, the chondrite-normalized PGE patterns (typically enriched in Os-Ir-Ru and distinct slope trends are lacking, instead exhibit a supergene enrichment of Pt and Pd relative to the total PGE (Figure 9a). In contrast, compact magnetite from Olympos has shown abundant chromite of homogeneous composition (high-Cr) surrounded by magnetite, but the dominant silicate mineral is serpentine, and PGE patterns resemble the negative slope of the PGE patterns for chromitites [3,9,28]. Therefore, the characteristic features described for compact magnetite from Skyros support an origin via a metamorphic process of re-deposited laterites, in contrast to that in Olympos, formed probably by transformation of chromite ore.

Below is a schematic summary (Figure 10) of metal potential pathways during the evolution from lateritization of ophiolites, re-deposition of laterite crusts on peridotites and metamorphism to compact magnetite.

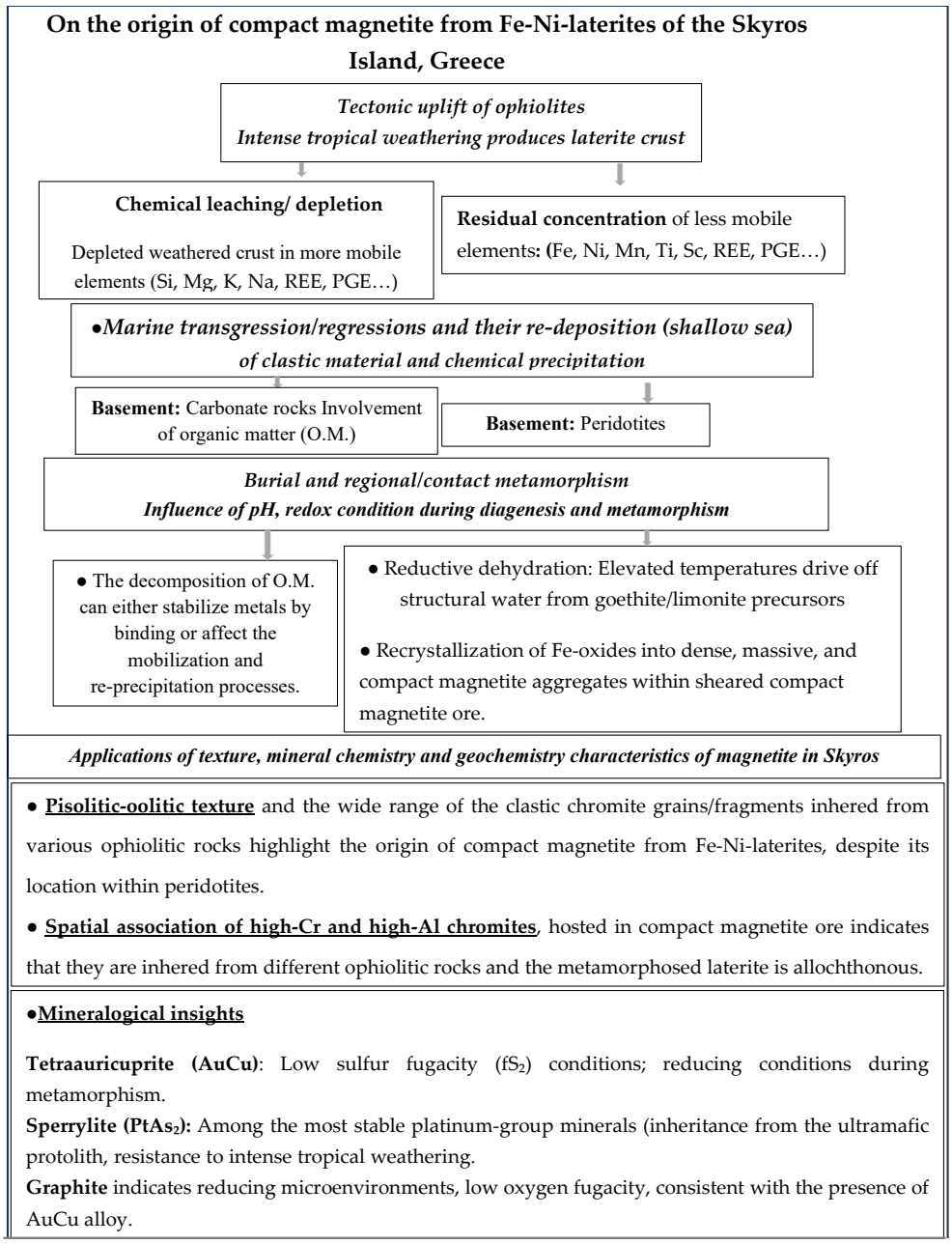


Figure 10. Conceptual multistage evolution proposed for the Skyros magnetite-bearing material.

6. Conclusions

The combination of the presented mineralogical and geochemical data in the present study may yield the following conclusions:

- Compact magnetite deposits hosted by peridotites can preserve texture, mineral chemistry, and geochemical fingerprints of a Fe–Ni laterite occurrence.
- Preserved pisolitic–oolitic textures, compositionally diverse high-Al to high-Cr chromite in a special association, and relatively flat-shaped PGE patterns collectively support derivation of the compact magnetite from a lateritic precursor.
- The relatively low content of critical elements (PGE, REE, Ni, Co, Sc) in the Skyros compact magnetite may be related to the transportation and re-deposition of laterite crusts onto peridotites and subsequently metamorphosed into compact magnetite ore under reducing conditions.

- Pentlandite and Co-bearing pentlandite hosted in compact magnetite reflect the preference of Ni and Co for sulfides and the limited capacity of magnetite to hold these metals in its crystal structure under certain metamorphic conditions.

Author Contributions: Conceptualization, M.E.-E. and C.K.; methodology, C.K.; software, C.K.; validation, M.E.-E. and C.K.; formal analysis, C.K. investigation, M.E.-E. and C.K.; resources, M.E.-E. and C.K.; data curation, M.E.-E. and C.K.; writing—original draft preparation, M.E.-E. and C.K.; writing—review and editing, M.E.-E. and C.K.; visualization, M.E.-E. and C.K.; supervision, M.E.-E. and C.K.; All authors have read and agreed to the published version of the manuscript.

Funding: This research received no external funding.

Data Availability Statement: The original contributions presented in this study are included in the article. Further inquiries can be directed to the corresponding author.

Acknowledgments: The authors gratefully acknowledge the staff of the Hellenic Survey of Geology and Mineral Exploration (HSGME) for their valuable assistance with sample preparation and analytical procedures. The consideration of this work and constructive suggestions by the anonymous reviewers are very much appreciated. The authors have reviewed and edited the output and take full responsibility for the content of this publication.

Conflicts of Interest: The authors declare no conflicts of interest.

References

1. Eliopoulos, D.G.; Economou-Eliopoulos, M. Trace Element Distribution in Magnetite Separates of Varying Origin: Genetic and Exploration Significance. *Minerals* **2019**, *9*, 759. [CrossRef]
2. Peters, S.T.M.; Feng, D.; Troll, V.R.; Pack, A.; Tornos, F.; Andersson, U.B.; Lehmann, B.; Di Rocco, T. Formation of iron oxide-apatite deposits triggered by magmatic assimilation of evaporitic sulfate. *Nat. Commun.* **2026**, *17*, 5930. [CrossRef] [PubMed]
3. Mitsis, I.; Economou-Eliopoulos, M. Occurrence of apatite with magnetite in an ophiolite complex (Othrys), Greece. *Am. Miner.* **2001**, *86*, 1143–1150. [CrossRef]
4. Paraskevopoulos, G.; Economou, M. Genesis of magnetite ore occurrences by metasomatism of chromite ores in Greece. *Neues. Jahrb. Mineral. Abh.* **1980**, *140*, 29–53.
5. Economou, M.I.; Naldrett, A.J. Sulfides associated with podiform bodies of chromite at Tsangli, Eretria, Greece. *Miner. Depos.* **1984**, *19*, 289–297. [CrossRef]
6. Foose, M.P.; Economou, M.; Panayiotou, A. Compositional and mineralogic constraints on the genesis of ophiolite hosted nickel mineralization in the Pevkos area, Limassol Forest, Cyprus. *Miner. Depos.* **1986**, *20*, 234–240. [CrossRef]
7. Kapsiotis, A.; Economou-Eliopoulos, M.; Zheng, H.; Huang, Q.; Lenaz, D.; Antonelou, A.; Velicogna, M.; Xia, B. Metallogeny of a base metal sulfide-bearing magnetitite body from the Eretria mine, East Othris massif, Greece: Insights into 108 an ancient seafloor hydrothermal system. *J. Geochem. Explor.* **2021**, *221*, 106703. [CrossRef]
8. Agiorgitis, G.; Wolf, R. Aspects of osmium, ruthenium and iridium contents in some Greek chromitites. *Chem. Geol.* **1978**, *3*, 267–272. [CrossRef]
9. Economou-Eliopoulos, M. Platinum-group element distribution in chromite ores from ophiolite complexes: Implications for their exploration. *Ore Geol. Rev.* **1996**, *11*, 363–381. [CrossRef]
10. Bussolesi, M.; Grieco, G.; Zaccarini, F.; Xiong, F.; Cavallo, A. The effect of multiple alteration processes on Skyros chromitites (Northern Sporades, Greece). *Ofioliti* **2025**, *50*, 1–16.
11. Stavropoulou, B. Metallogeny of Mafic-Ultramafic Rocks from Slyrow Island. Diploma Thesis, University of Athens, Athens, Greece, 1987; p. 150.
12. Valeton, I.; Biermann, M.; Reche, R.; Rosenberg, F. Genesis of Nickel laterites and bauxites in Greece during the Jurassic and Cretaceous, and their relation to ultrabasic parent rocks. *Ore Geol. Rev.* **1987**, *2*, 359–404. [CrossRef]
13. Alevizos, G. Mineralogy, Geochemistry and Origin of the Sedimentary Fe–Ni Ores of Lokris. Ph.D. Thesis, Technical University of Crete, Chania, Greece, 1997; p. 245.
14. Thorne, R.; Herrington, R.J.; Roberts, S. Composition and origin of the Çaldăg oxide nickel laterite, W. Turkey. *Miner. Depos.* **2009**, *44*, 581–595. [CrossRef]
15. Economou-Eliopoulos, M.; Laskou, M.; Eliopoulos, D.G.; Megremi, I.; Kalatha, S.; Eliopoulos, G.D. Origin of critical metals in Fe–Ni laterites from the Balkan Peninsula: Opportunities and environmental risk. *Minerals* **2021**, *11*, 1009. [CrossRef]

16. García-Tudela, M.; Aiglsperger, T.; Proenza, J.A.; Racek, M.; Gorzsás, A.; Longo, F. Speculations on the genesis of enigmatic Pt-Ir-Fe-Ni micro-nuggets from the Falcondo Ni-laterite deposit, Dominican Republic. *Miner. Depos.* **2026**, *61*, 1597–1624. [CrossRef]
17. Lewicka, E.; Guzik, K.; Galos, K. On the Possibilities of Critical Raw materials Production from the EU's Primary Sources. *Resources* **2021**, *10*, 50. [CrossRef]
18. Mountrakis, D. Introduction to the geology of Macedonia and Trace: Aspects of the geotectonic evolution of the Hellenides. *Bull. Geol. Soc. Greece* **1992**, *30*, 31–46.
19. Jacobshagen, G.; Matarangas, D. Nappe structure of the North Sporades (Greece): On the geological evolution of Alonissos island. *Bull. Geol. Soc. Greece* **2004**, *36*, 1636–1642. [CrossRef]
20. Harder, H.; Jacobshagen, V.; Skala, W.; Arafeh, M.; Berndsen, J.; Hofmann, A.; Kusserow, H.; Schedler, W. Geologische Entwicklung und Struktur der Insel Skyros, Nordsporaden, Griechenland. *Berl. Geowiss. Abh.* **1983**, *48*, 7–40.
21. Pe-Piper, G.; Matarangas, D.; Jacobshagen, V. The Mesozoic metavolcanics rocks of Alonnisos and Kyra Panagia islands, Sporades, Greece. *N. Jb. Miner. Mh.* **1996**, *6*, 251–263.
22. Karkalis, C.; Magganas, A.; Koutsovitis, P. Petrological, mineralogical and geochemical data from the Eohellenic ophiolitic nappe in the island of Skyros, Greece. In Proceedings of the Bulletin of the Geological Society of Greece, Proceedings of the 14th International Congress, Thessaloniki, Greece, 25–27 May 2016; pp. 1867–1877.
23. Papanikolaou, D. Timing of tectonic emplacement of the ophiolites and terrane paleogeography in the Hellenides. *Lithos* **2009**, *108*, 262–280. [CrossRef]
24. Boundi, D.; Papanikolaou, D.; Bosio, G.; Montemagni, C. Late Cretaceous Tectono-Metamorphic Events in the Skyros Upper Metamorphic Unit (Olympus Mountain), Aegean Sea, Greece. *Geosciences* **2024**, *14*, 69. [CrossRef]
25. Babechuk, M.G.; Widdowson, M.; Kamber, B.S. Quantifying chemical weathering intensity and trace element release from two contrasting basalt profiles, Deccan Traps, India. *Chem. Geol.* **2014**, *363*, 56–75. [CrossRef]
26. Barrat, J.A.; Bayon, G.; Lalonde, S. Calculation of cerium and lanthanum anomalies in geological and environmental samples. *Chem. Geol.* **2023**, *615*, 121202. [CrossRef]
27. Eliopoulos, D.; Economou-Eliopoulos, M. Geochemical and mineralogical characteristics of Fe–Ni and bauxitic–laterite deposits of Greece. *Ore Geol. Rev.* **2000**, *16*, 41–58. [CrossRef]
28. Economou-Eliopoulos, M. Apatite and Mn, Zn, Co-enriched chromite in Ni-laterites of northern Greece and their genetic significance. *J. Geochem. Explor.* **2003**, *80*, 41–54. [CrossRef]
29. Aiglsperger, T.; Proenza, J.A.; Lewis, J.F.; Labrador, M.; Svojtka, M.; Rojas-Purón, A.; Longo, F.; Ďurišová, J. Critical metals (REE, Sc, PGE) in Ni laterites from Cuba and the Dominican Republic. *Ore Geol. Rev.* **2016**, *73*, 127–147. [CrossRef]
30. Aiglsperger, T.; Proenza, J.A.; Font-Bardia, M.; Baurier-Amat, S.; Gali, S.; Lewis, J.F.; Longo, F. Supergene neoformation of Pt-Ir-Fe-Ni alloys: Multistage grains explain nugget formation in Ni-laterites. *Mineral. Depos.* **2017**, *52*, 1069–1083. [CrossRef]
31. Al-Khirbash, S.; Semhi, K.; Richard, L.; Nasir, S.; Al-Harthy, A. Rare earth element mobility during laterization of mafic rocks of the Oman ophiolite. *Arab. J. Geosci.* **2024**, *7*, 5443–5454.
32. Goutzioura, K. Mineralogy and Geochemistry of Agios Ioannis, Larymna, Greece (LARCO GMMSA) Ni-Laterite. Master's Thesis, University of Athens, Athens, Greece, 2021; p. 139.
33. Golightly, J.P. Progress in understanding the evolution of nickel lateritics. In *The Challenge of Finding New Mineral Resources—Global Metallogeny, Innovative Exploration, and New Discoveries*; Goldfarb, R.J., Marsh, E.E., Monecke, T., Eds.; Economic Geology. Special Publication 15; Society of Economic Geologists, Inc.: Littleton, CO, USA, 2010; Volume 15, pp. 451–486.
34. Irzon, R. Element mobilization during weathering process of ultramafic complex in North Konawe Regency, Southeast Sulawesi based on a profile from Asera. *Indones. J. Geosci.* **2018**, *5*, 277–290. [CrossRef]
35. Gruau, G.; Bernard-Griffiths, J.; Lécuyer, C. The origin of U-shaped rare earth patterns in ophiolite peridotites: Assessing the role of secondary alteration and melt/rock reaction. *Geochim. ET Cosmochim. Acta* **1998**, *62*, 545–3560. [CrossRef]
36. Konstantopoulou, G.; Economou-Eliopoulos, M. Distribution of Platinun-Group Elements and Gold within the Vourinos chromitite ores, Greece. *Econ. Geol.* **1991**, *86*, 1672–1682. [CrossRef]
37. Laskou, M.; Economou-Eliopoulos, M. Bio-mineralization and potential biogeochemical processes in bauxite deposits: Genetic and ore quality significance. *Miner. Petrol.* **2013**, *107*, 471–486. [CrossRef]
38. Economou-Eliopoulos, M.; Kalatha, S. Potential pathways for lithium and Cr-isotopes during biogeochemical redox processes: Insights from karst-type laterites of Greece. *Chem. Geol.* **2025**, *687*, 122865. [CrossRef]
39. Rivera, J.; Reich, M.; Schoenberg, R.; Gonz'alez-Jim'enez, J.M.; Barra, F.; Aiglsperger, T.; Proenza, J.A.; Carretier, S. Platinum-group element and gold enrichment in soils monitored by chromium stable isotopes during weathering of ultramafic rocks. *Chem. Geol.* **2018**, *499*, 84–99. [CrossRef]
40. Bowles, J.F.W. The development of platinum-group minerals in laterites. *Econ. Geol.* **1986**, *81*, 1278–1285. [CrossRef]
41. Bowles, J.F.W.; Suárez, S.; Prichard, H.M.; Fisher, P.C. Weathering of PGE-sulfides and Pt-Fe alloys, in the Freetown Layered Complex, Sierra Leone. *Miner. Depos.* **2017**, *52*, 1127–1144. [CrossRef]

42. Kalatha, S.; Perraki, M.; Economou-Eliopoulos, M.; Mitsis, I. On the origin of bastnaesite-(La, Nd, Y) in the Nissi (Patitira) bauxite laterite deposit, Lokris, Greece. *Minerals* **2017**, *7*, 45. [CrossRef]
43. Teitler, Y.; Favier, S.; Ambrosi, J.-P.; Sevin, B.; Golfier, F.; Cathelineau, M. Evaluation of Sc Concentrations in Ni-Co Laterites Using Al as a Geochemical Proxy. *Minerals* **2022**, *12*, 615. [CrossRef]
44. Tarkian, M.; Economou-Eliopoulos, M.; Eliopoulos, D. Platinum-group minerals and tetra-auricuprite in ophiolitic rocks of the Skyros Island, Greece. *Mineral. Petrol.* **1992**, *47*, 55–66. [CrossRef]

Disclaimer/Publisher's Note: The statements, opinions and data contained in all publications are solely those of the individual author(s) and contributor(s) and not of MDPI and/or the editor(s). MDPI and/or the editor(s) disclaim responsibility for any injury to people or property resulting from any ideas, methods, instructions or products referred to in the content.